ORIGINAL ARTICLE

Impact of claudin-10 deficiency on amelogenesis: Lesson from a HELIX tooth

Nicolas Obtel[1,2] | **Adeline Le Cabec**[3,4] | **Thè Nghia Nguyen**[1] | **Eloise Giabicani**[1] | **Stijn J. M. Van Malderen**[5] | **Jan Garrevoet**[5] | **Aline Percot**[6] | **Céline Paris**[6] | **Christopher Dean**[7,8] | **Smail Hadj-Rabia**[9] | **Pascal Houillier**[10,11] | **Tilman Breiderhoff**[12] | **Claire Bardet**[1] | **Thibaud Coradin**[13] | **Fernando Ramirez Rozzi**[1,14] | **Catherine Chaussain**[1,2]

[1]Université Paris Cité, URP2496 Pathologies, Imagerie et Biothérapies Orofaciales et Plateforme Imagerie du Vivant (PIV), FHU-DDS-net, IHMOA, Dental School, Montrouge, France

[2]AP-HP Services de médecine bucco-dentaire, Hôpitaux Universitaires Bretonneau (CRMR phosphore et calcium, filière OSCAR et ERN Bond) and Charles Foix, FHU DDS-net, Ile de France, France

[3]Univ. Bordeaux, CNRS, MCC, PACEA, UMR 5199, Pessac, France

[4]Department of Human Evolution, Max Planck Institute for Evolutionary Anthropology, Leipzig, Germany

[5]Deutsches Elektronen-Synchrotron DESY, Hamburg, Germany

[6]Sorbonne Université, CNRS, De la Molécule aux Nano-Objets: Réactivité, Interactions et Spectroscopies (MONARIS), Paris, France

[7]Department of Earth Sciences, Centre for Human Evolution Research, Natural History Museum, London, UK

[8]Department of Cell and Developmental Biology, University College London, London, UK

[9]Université Paris Cité, INSERM1163 Institut Imagine; APHP, Hôpital Necker-Enfants Malades, Department of Dermatology, Reference Center for Rare Skin Diseases, Paris, France

[10]Université Paris Cité, Sorbonne Université, Centre de Recherche des Cordeliers, INSERM, CNRS-ERL8228, Paris, France

[11]APHP, Service de Physiologie, Centre de Référence des Maladies Rénales Héréditaires de l'Enfant et de l'Adulte (MARHEA), Hôpital Européen Georges Pompidou, Paris, France

[12]Charité Universitaetsmedizin Berlin, Division of Gastroenterology, Nephrology and Metabolic Diseases, Department of Pediatrics, Berlin, Germany

[13]Sorbonne Université, CNRS, Laboratoire de Chimie de la Matière Condensée de Paris, Paris, France

[14]Eco-anthropologie (EA), Muséum national d'Histoire naturelle, CNRS, Université de Paris, Paris, France

Correspondence
Catherine Chaussain, URP2496, Université Paris Cité, 1 rue Maurice Arnoux, 92120 Montrouge, France.
Email: catherine.chaussain@u-paris.fr

Nicolas Obtel and Adeline Le Cabec contributed equally to this work.

Abstract

In epithelia, claudin proteins are important components of the tight junctions as they determine the permeability and specificity to ions of the paracellular pathway. Mutations in *CLDN10* cause the rare autosomal recessive HELIX syndrome (Hypohidrosis, Electrolyte imbalance, Lacrimal gland dysfunction, Ichthyosis, and Xerostomia), in which patients display severe enamel wear. Here, we assess whether this enamel wear is caused by an innate fragility directly related to claudin-10 deficiency in addition to xerostomia. A third molar collected from a female HELIX patient was analyzed by a combination of microanatomical and physicochemical approaches

(i.e., electron microscopy, elemental mapping, Raman microspectroscopy, and synchrotron-based X-ray fluorescence). The enamel morphology, formation time, organization, and microstructure appeared to be within the natural variability. However, we identified accentuated strontium variations within the HELIX enamel, with alternating enrichments and depletions following the direction of the periodical striae of Retzius. These markings were also present in dentin. These data suggest that the enamel wear associated with HELIX may not be related to a disruption of enamel microstructure but rather to xerostomia. However, the occurrence of events of strontium variations within dental tissues might indicate repeated episodes of worsening of the renal dysfunction that may require further investigations.

INTRODUCTION

In mammals, tooth enamel is the most mineralized structure of the organism and forms the outer layer of the dental crown. Amelogenesis is a complex process that occurs before tooth eruption. It results from a complex epithelial–mesenchymal cross-talk between the ectoderm-derived enamel organ and the neural crest-derived dental mesenchyme.[1–4] Enamel synthesis encompasses two major steps, namely, the secretory stage during which the ameloblasts, the enamel-secreting cells of the enamel organ, secrete a template of enamel-specific extracellular matrix proteins, and the maturation stage during which most of this scaffold is replaced by hydroxyapatite.[5–9] Two types of maturation ameloblasts are reported according to morphological criteria.[9,10] Ruffle-ended ameloblasts exhibit a distal plasma membrane with multiple invaginations, whereas smooth-ended ameloblasts display a smooth distal membrane. These two cell types alternate during the maturation process and the pH of the associated enamel matrix from 6.2 for ruffle-ended ameloblasts to 7.2 for smooth-ended ameloblasts.[9,11,12]

At the secretory stage, ameloblasts display a double set of tight junctions (TJs), both at their apical and basal ends. At the maturation stage, smooth-ended ameloblasts remove their apical TJs, whereas they reform in ruffle-ended ameloblasts.[9,10,13] Claudin proteins are the main components of the TJs that are either sealing the paracellular space or forming a pore, thus determining their permeability and ion specificity.[14] The expression of several claudins has been reported in the secretory ameloblast TJs,[15] including claudin-1, -3, -16, and -19,[10,16–18] whereas claudin-16 was not found in maturation ameloblasts.[16] Claudin-10 was shown to be expressed in the enamel organ and more precisely in the stratum intermedium, a layer of epithelial cells located immediately adjacent to the basal end of the ameloblast layer.[19] Two isoforms of claudin-10 are expressed in the kidney,[20] claudin-10a and claudin-10b. The expression of claudin-10a, which is anion-selective, is restricted to the proximal tubule.[21] Claudin-10b, which is cation-selective and may determine paracellular sodium

permeability,[22,23] is expressed not only in the thick ascending limb of Henle's loop in the kidney[21] but also in other epithelia.[24,25]

Several genetic disorders affect the enamel structure of all the teeth from both dentitions, resulting in *Amelogenesis imperfecta* manifested by severe dental defects, which require complex restorations and significantly alter a patient's quality of life.[4,5,26–29] Among them, nonsyndromic *Amelogenesis imperfecta* are due to pathogenic variants of genes that encode enamel-specific extracellular matrix proteins (*AMELX, ENAM,* and *AMBN)*, or proteins involved in enamel maturation (*MMP20, KLK4,* and *SLC24A4*), or cell–cell and cell–matrix attachments (*ITGB6, COL17A1, LAMA3,* and *LAMB3*).[26,30]

Amelogenesis imperfecta is also frequently found in patients with genetic disorders related to kidney, skin, and other organs.[16,26,30,31] A disorder of this sort was recently found to be associated with loss-of-function variants of *CLDN10*, resulting in the autosomal recessive HELIX syndrome characterized by hypohidrosis, electrolyte imbalance, lacrimal gland dysfunction, ichthyosis, and xerostomia (OMIM 617671; prevalence: <1/1,000,000).[32–37] In addition, it has been reported that the patients with HELIX syndrome displayed a very early and severe enamel wear.[34] At the time of examination, it was difficult to determine whether this severe enamel wear mainly resulted from erosion due to the impaired salivary secretion,[32] or from enamel fragility directly related to claudin-10 deficiency, as claudin-10 is expressed in the forming tooth germ.[15,19] In the present study, the examination of the enamel of a retained third permanent molar, which was in a submucosal position and, therefore, partially exposed to the oral environment, was used to explore this question. The tooth was removed for orthodontic therapeutic reasons from a young female adult patient with HELIX syndrome. By combining microanatomical and physico-chemical approaches, we showed that neither the rate of enamel formation nor its morphology, organization, and structure were significantly impacted by claudin-10 deficiency. However, we identified the occurrence of random events of strontium variations within both enamel and dentin that may reflect a disorder in strontium handling, potentially caused by the renal dysfunction.

MATERIALS AND METHODS

Samples

An impacted right permanent third lower molar was collected from a 19-year-old female patient with the HELIX syndrome. This patient was already reported as patient A-IV-2.[34] This family presented a missense variation c.386C >T (NM_182848), p.S129L in claudin-10a (c.392C> T (NM_006984), and p.S131L in claudin-10b. A 3D cone beam computed tomography (CBCT) exam of the lower jaw was performed to prepare the surgery. Since this impacted third molar displayed severely curved roots, the surgeon decided to section it to limit postoperative adverse events. Three impacted age-matched third molars were gathered and were randomly used as control for the various experiments. All teeth were extracted at the request of an orthodontist in the context of a treatment plan and were collected with the informed consent of the patients, in accordance with the ethical guidelines laid down by French law (agreement IRB 00006477 and n° DC-2009-927, Cellule Bioéthique DGRI/A5). All teeth were fixed in 70% ethanol for a week.

Preparation of the tooth sections

Sections of the crown of the HELIX patient's molar and control third molars were carried out to study the microanatomy of dental tissues by optical and scanning electron microscopy (SEM) and to perform chemical analyses by Raman microspectroscopy, energy-dispersive-X-ray (EDX) microanalysis and synchrotron X-ray fluorescence (SXRF) imaging. For the HELIX molar, since the distal half of the crown came as a fragment and was, therefore, more difficult to handle although it preserved both enamel and dentin, the section was performed on that fragment, thus yielding a bucco-distal crown thin section. A bucco-lingual section through the mesial cusps was performed on the control lower third molars.

For preparation of the thin sections for microanatomy, Raman, and SXRF analyses, the teeth were embedded in cyanoacrylate and fixed with wax on the glass slide. We used a saw equipped with a diamond disk (Struers, Champigny-sur-Marne, France) under a continuous water spray. After the first cut, the surface of the block was polished with carbide grinding paper (Grit 600/P1200) and Chemomet paper with 1 μm aluminum powder (Bühler, Uzwil, Switzerland). This surface was glued onto the slide with Araldite 2020 (Huntsman Corporation, The Woodlands, TX, USA). The block was then sectioned into ~300 μm slices and polished (Grit 600/P1200) to reach an average thickness of ~160 μm for the HELIX molar and ~60 μm for the control third molar. The polishing process was kept minimal for the HELIX tooth because of its smaller size. Finally, the sections were polished again with Chemomet paper with 1 μm aluminum powder until a completely flat surface was obtained.

For preparation of the sections for SEM and EDX analyses, 1 mm-thick sections in mirror of the control and HELIX third molars were prepared with a saw equipped with a diamond disk (Struers) under a continuous water spray. For SEM analysis, after thorough polishing, surfaces were cleaned with 5% sodium hypochlorite under ultrasonic activation for 2 min, rinsed twice with distilled water, etched with 36% orthophosphoric acid (DeTrey® Conditioner 36, Dentsply Sirona, York, PA, USA) for 12 s, and then thoroughly rinsed with distilled water. For EDX analysis, after polishing, surfaces were cleaned under ultrasonic activation for 2 min and rinsed twice with distilled water.

Study of the microanatomy of dental tissues

The HELIX crown section was mounted on a glass slide for observation and analysis. The section was analyzed using incident light with a stereomicroscope Leica M8 and transmitted light with a Zeiss Universal photomicroscope. The Zeiss microscope was fitted with an Idea camera connected to a computer using Spot software (Version 5.4). The images were processed with Nikon ViewN2 and their analysis was performed with ImageJ.

Analysis of the dental microanatomy allows the study of the daily secretion rate (DSR) of the enamel and the formation time of the crown thanks to the presence of periodical growth lines in the enamel, the cross-striations, and the striae of Retzius (Figure S1). Cross-striations reflect the circadian variation of the enamel secretion, their spacing is indicative of the amount of enamel formed per day and yields the DSR.[38] The striae of Retzius, which correspond to longer successive steps of enamel formation, are formed at regular intervals. Their periodicity is determined by counting the number of cross-striations in between two successive striae. This periodicity is assumed to be constant during the entire crown formation time of a given tooth. According to the arrangement of Retzius' striae in the enamel, the dental crown can be divided into a cuspal part, located at the occlusal third of the tooth, in which striae are arranged in successive arches around the dentin horn and a lateral part, which is formed subsequently and until crown completion at the cervix[39] (Figure S1). In the lateral enamel, striae of Retzius crop out and terminate at the surface of the enamel rather than arch over the dentin horn.

The DSR was obtained in the cuspal portion of the crown near the apparent dentin horn (Figure S1). A line running along the direction of an enamel prism between the enamel–dentin junction (EDJ) and the outer enamel surface (OES) was then divided into 100 μm-thick zones to calculate DSR changes during the course of crown formation.[40,41] In each zone, the average spacing between cross-striations was measured. This was performed several times in each zone, always across a minimum number of three cross-striations, in order to obtain an average DSR for each zone, and finally to calculate an overall average DSR for the cuspal enamel. The total cuspal enamel formation time is equal to the thickness of cuspal enamel divided by the average daily cross-striations spacing.

To describe the development of the lateral enamel, the height of the crown, taken between the cusp tip and the enamel cervix, was divided into deciles of crown height.[42] Noticeably, in the first two deciles, striae were difficult to distinguish so that the formation time was estimated

by dividing the length of the prism path between the limit cuspal-lateral enamel and the first striae of the third decile by the DSR of this area. The number of striae of Retzius was counted within each decile and multiplied by their periodicity. Periodicity was obtained in three locations. The lateral enamel formation time is equal to the total count of Retzius lines multiplied by their periodicity, that is, 8 days (Figure 1E). The crown formation time was obtained by the sum of cuspal and lateral enamel formation times (Figure S1).

SEM imaging and EDX analyses

For SEM imaging, thick sections of the HELIX and control third molars were coated with a thin gold layer (∼30 nm) using a CRESSINGTON 108 AUTO gold sputter coater. For EDX measurements, the thick sections were coated with a thin layer of carbon (∼ 20 nm) by evaporation using a CRESSINGTON 208C carbon coater. Imaging and analysis were performed at 15 kV at different magnifications using a Hitachi SU-70 microscope equipped with a Field Emission Gun. All the samples were evaluated for Ca, P, and Mg content (% atom) in the outer and inner layers of enamel, and at least three measurements were performed for each layer.

Raman microspectroscopy

Raman analyses were performed using a Senterra Raman microspectrometer (Bruker Optics), using a laser emitting at 785 nm settled to provide a laser power at the sample of about 25 mW. Data collection was controlled by the OPUS 7.5 software (Bruker Optics). Measurements were collected across one spectral window (450–1800 cm^{-1}) at a spectral resolution of about 3 cm^{-1}, and each analysis was the coaddition of two spectra accumulated at up to 30 s of exposure time for each. Analyses were performed using a 50× objective (Olympus, Tokyo, Japan), giving an analytical spot size of approximately 12 μm in diameter, with the used excitation wavelength. Analyses were directly performed on polished surfaces of the thin sections. For mapping, the sample was moved by a computer-controlled stage. Each surface was scanned by moving the sample by about 18 μm steps. Maps were performed on a 700 × 2150 μm surface for the control sample and 1000 × 1850 μm surface for the HELIX sample. Chemical maps were generated by integrating the area of the band centered at 1070 cm^{-1} (I_{1070}) and the band centered at 960 cm^{-1} (I_{960}), attributed to the vibration of carbonate ($\nu(CO_3^{2-})$) and phosphate ($\nu(PO_4^{3-})$) groups in the mineral phase, respectively.[43] Ratios between both maps were done to monitor the chemical distribution. Maps have been depicted using the same color scheme. Full width at half maxima (FWHM) with imposed fitted position was also determined. Maps based on the $\nu(PO_4^{3-})$ full width at half maxima (FWHM$_{960}$) for both samples were also presented with a color scale going from 10 to 16 cm^{-1}. Baseline subtractions, fitting, and map generation were managed by the OPUS 8.7 software (Bruker Optics).

Synchrotron X-ray fluorescence data acquisition and processing

SXRF analysis was performed on the P06 Beamline,[44,45] Petra III, at DESY (Deutsches Elektronen-Synchrotron, Hamburg, Germany), a member of the Helmholtz Association HGF. Both the HELIX third molar and the control third molar were scanned. The thin section of the HELIX molar was left mounted on a glass slide support, while the control molar was mounted on suspended kapton foil. The storage ring was operated in 480-bunch mode in top-up filling mode with an average current of 120 mA ± 0.5 mA. The primary X-ray beam was monochromatized to 16.6 keV using a double crystal Si111 monochromator and focused using a Kirkpatrick–Baez mirror system (JTEC, Japan) to approximately 500 × 500 nm^2. The experimental configuration consisted of two Vortex EM silicon drift detectors (Hitachi High-Tech Science America, Inc.), the second of which was collimated. Both detectors were positioned symmetrically at scattering angles of 135 degrees at a distance of 9 mm from the focal point at the sample surface. The use of dual-detector "backscatter" geometry maximizes the solid angle during the analysis of thin polished samples (∼110 μm-thick on average in this study), and allows large area to be scanned with micrometric resolution using millisecond dwell times.[46] This setup allowed capturing Kα emission lines from Si to Sr, with varying detection efficiency.

Spectral peak deconvolution and integration were performed using the core of PyMca 5.5.0.[47] Image analysis was performed in HDIP v-1.3.3.1073 (Teledyne CETAC Technologies, Bozeman, MT, USA). The X-ray yield calculations were performed using an in-house script assuming a hydroxyapatite matrix ($Ca_{10}(PO_4)_6(OH)_2$) with density 2.85 g/cm^3 for the enamel phase and 1.6 g/cm^3 for the dentin phase.[48] Elemental mass fractions were determined by calculating an areal density sensitivity from measurements standard Ti, Fe, and Cu foils with an areal density of 59.0, 55.0, and 47.9 μg/cm^2, respectively (Micromatter Technologies Inc., Canada), and measured thickness of the samples. Tooth section thickness was measured throughout the whole surface of the specimens in four positions for HELIX and five positions for the control tooth. The average tooth section thickness (160 and 61 μm, respectively) was also taken into account in the X-ray mass attenuation coefficients of the hydroxyapatite phase during attenuation correction.[49] Glass slides and kapton foil substrates were included in the overall sample model as appropriate (i.e., background subtraction). Normalization to the incoming X-ray flux was applied. In the calibrated data, SXRF concentrations are reported by mass fraction (μg.g^{-1}, i.e., ppm), and/or areal density (g.cm^{-3}).

A multiscale scanning strategy was used to optimize efficiency. First, a fast overview scan was acquired at 100 μm (dwell time: 10 ms) to check that the tooth section is well-centered in the field of view, and assess the overall signal of the dental tissues. Then, a middle resolution (MR) overview scan allowed visualizing the elemental variation within the entire tooth section (i.e., enamel and dentin). The HELIX third molar section was scanned at 10 μm with 3 ms dwell time (X = 6.31 mm × Y = 6.44 mm, t = 33 min). The control third molar section was scanned at 10 μm, with 3 ms dwell time (X = 18.35 mm × Y = 7.99 mm,
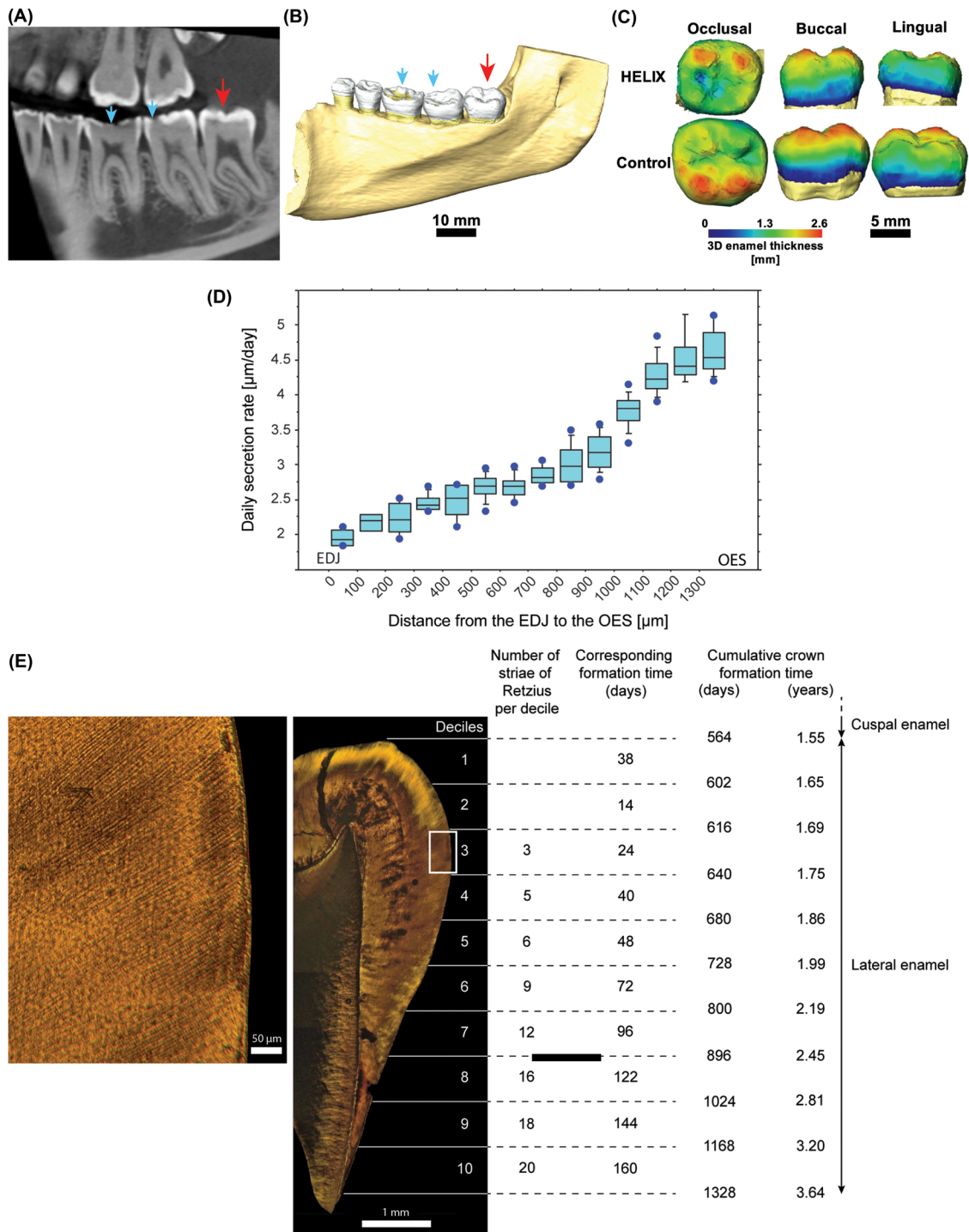
FIGURE 1 Anatomy and microanatomy of the HELIX molar. (A,B) Cross-section of CBCT image (A) and 3D reconstruction (B) of the right lower jaw of the female HELIX patient. The partially erupted third molar (red arrow) shows an unworn and normally formed enamel, whereas the erupted molars display occlusal wear (blue arrows). (C) 3D reconstructions of the third molar crowns, showing that the HELIX enamel has a comparable 3D enamel thickness distribution to the control. (D) Determination of the daily secretion rate (DSR) in the HELIX enamel. The DSR (µm/day) increases from the enamel–dentin junction (EDJ) to the outer enamel surface (OES). (E) Quantification of the HELIX crown formation time. The cuspal enamel took 564 days (1.55 years) to form. The number of striae of Retzius and corresponding days of formation (days) are given for each decile of the lateral enamel. The total crown formation time is 1328 days (3.64 years). The area of interest symbolized by the white rectangle in the middle image is at higher magnification in the left image. See Figure S1 for details about the methodology.

$t = 1.3$ h). Finally, based on prior observations of the HELIX tooth section under the microscope and the MR scans, two small regions of interest (ROI) were selected for acquiring high-resolution (HR) scans: at 1.5 µm (dwell time = 4 ms): (1) across the lateral enamel just below the end of the cuspal enamel (ROI: $X = 1.45$ mm $\times Y = 0.37$ mm, $t = 18$ min), and (2) across the EDJ roughly under the center of the occlusal basin (ROI: $X = 1.21$ mm $\times Y = 0.68$ mm, $t = 28$ min). No HR scan was acquired on the control molar, due to a normal and monotonous signal in the MR scan. Visualization and analysis of the SXRF data were performed in HDIP. The color-coded elemental maps were saved as 32-bit tiffs allowing for a fine-tuning of the contrast and brightness in ImageJ[50,51] to better reveal the stress pattern. To note that to denoise the images, a 2D Gauss filter was applied with a kernel size of 0.8×0.8.

Variations in Sr content

Since the chronology of the crown formation was established, any variation in Sr concentration could be given a time relative to the initiation of crown formation. Each significant variation (i.e., enrichment or depletion) in Sr content was allocated a letter, their distance from the EDJ was measured, and their chronological order of formation calculated. The timing of the changes in Sr content between the EDJ and the enamel surface along a transect was quantified using the same methodology as used in the cuspal enamel, that is, the cumulative length of the prism between the two reference points was divided by the average DSR of the concerned area.

RESULTS

Physiopathological condition and phenotype of the HELIX patient

The HELIX patient is a 19-year-old French female (patient A-IV-2) born at full term from consanguineous parents, and was raised in France.[34] She displayed xerosis of the skin with keratosis pilaris of cheeks, arms, thighs with a slight palmo-plantar keratoderma, and xerostomia. As presented in Hadj-Rabia et al.,[34] she had normal serum calcium, high serum magnesium, low serum potassium concentrations, and hypocalciuria. The patient underwent an orthodontic treatment between 12 and 14 years of age and, at the time of dental examination, exhibited a metallic orthodontic retainer at the lower jaw from canine to canine. As shown by the clinical examination, the orthopantomogram[34] and the CBCT examination (Figure 1A–C) of the right lower jaw, the patient exhibited severe enamel wear on all of her erupted teeth (blue arrows, Figure 1A,B). The crown of the third lower molar was fully formed although retained in a submucosal position and partially erupted into the oral cavity and displayed a normal morphology (red arrow, Figure 1A,B). In spite of the relatively low resolution of the CBCT scan (200 µm), the enamel thickness indices of the HELIX molar could be calculated on a virtual 2D section taken through the

mesial cusps in the developmental plane (Figure 1C and Supplementary Information). These indices were within the range of the published values for modern human permanent third molars,[52,53] suggesting that the volume of formed enamel was not disturbed by claudin-10 deficiency. Furthermore, CBCT showed that this third molar displayed an almost completed root formation and exhibited an enamel carious lesion located in the mesial fissure of the occlusal aspect (red arrow, Figure 1A).

Daily secretion rate and crown formation time in the HELIX molar

The average DSR for each 100-µm area in the HELIX molar is presented in Table S1. As shown in Figure 1D, the DSR increased from 1.96 µm/day in the inner zone of enamel near the EDJ to 4.62 µm/day in the outer zone of enamel near the enamel surface. The values and the pattern of the DSR for this HELIX third molar were similar to those reported for any normal human tooth.[54–56]

The total crown formation time of the HELIX tooth was then established (Figure 1E). For this tooth, we determined that the formation time of the cuspal enamel was 564 days. The periodicity of the striae of Retzius was 8 days. The number of striae in each decile of the lateral enamel is given in Figure 1E. The first two deciles corresponded to 52 days, while decile 3 to decile 10 contain 89 striae of Retzius formed over 712 days. The crown formation time was, therefore, 1328 days (3.64 years). The number of striae increased toward the cervix, from three striae in decile 3 (cusp tip) to 20 striae in decile 10 (cervix), indicating that the number of days within each decile increased toward the cervix (Figure 1E). In other words, the rate of crown lengthening slowed down from cusp tip to cervix. The pattern of striae of Retzius spacing among each of the deciles, as well as the formation time within each decile, and the overall crown formation time found in the HELIX third-molar were similar to those already established for healthy modern human third molars.[42]

Enamel microstructure of the HELIX tooth

We next investigated whether the microstructural characteristics of the enamel were affected by the HELIX syndrome. SEM observation showed that the enamel was correctly organized in HELIX when compared to control (Figure 2A,B). The enamel rods were perfectly formed and aligned in both cases (Figure 2C–F). Quite remarkably, the cross-striations, which correspond to the circadian variation in enamel apposition,[38] were particularly well-distinguishable in the HELIX rods (Figure 2E, black arrow-head), which may suggest a potential difference in the enamel content in HELIX. However, we cannot exclude that such variation may result from the sample processing, even if both teeth were prepared by the same operator, at the same time, and in the same conditions.[57]
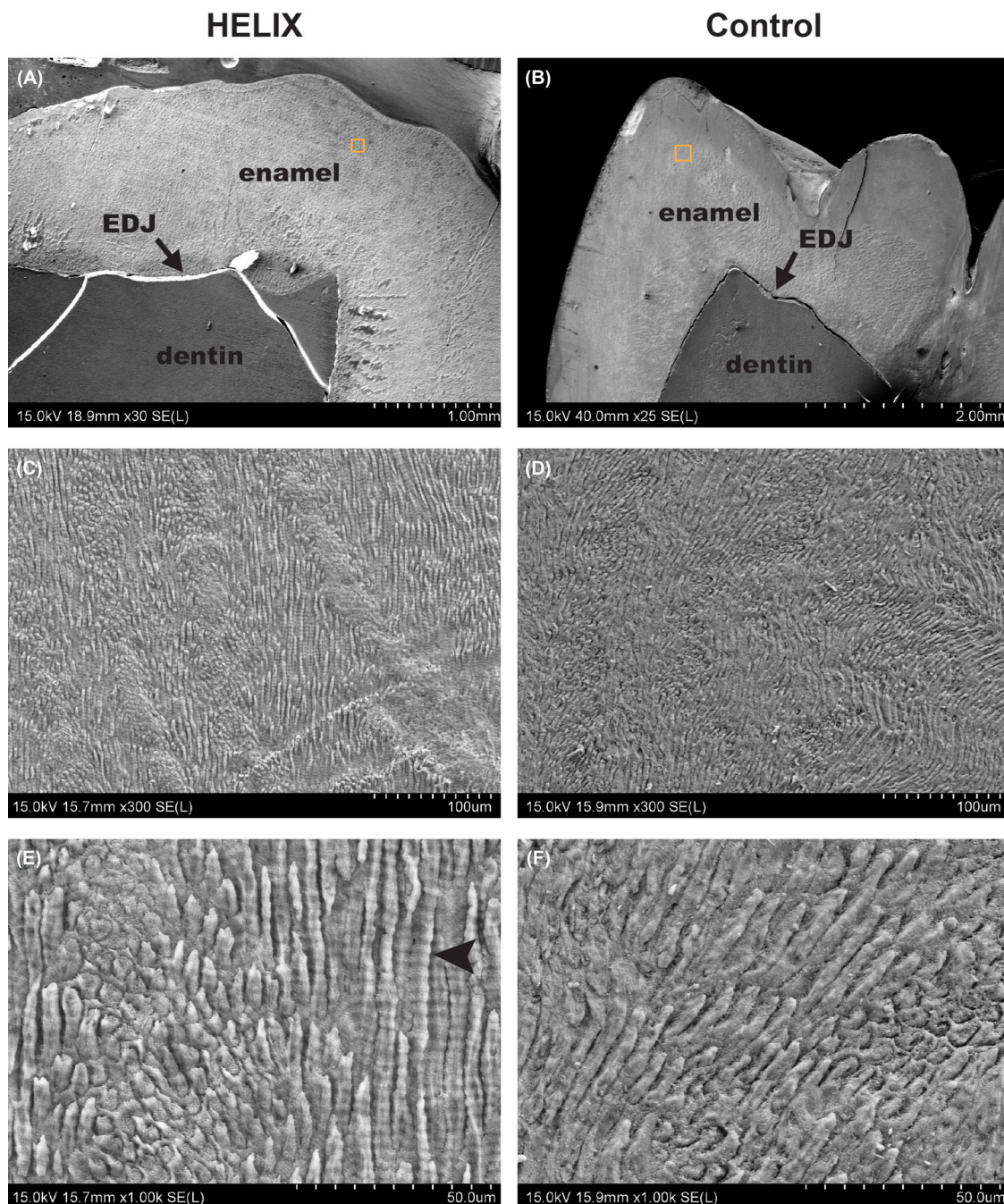
HELIX

Control

FIGURE 2 Characteristics of the HELIX enamel by SEM. (A–F) Representative aspects of the HELIX and control enamel microstructure imaged by SEM at various magnifications (A, B: ×25–30, C, D: ×300, E, F: ×1000, respectively). There is no difference between the HELIX enamel and the control enamel. Note that in the HELIX enamel, cross-striations are particularly well-distinguishable (E, black arrowhead). Abbreviation: EDJ, enamel–dentin junction.

Crystallinity and carbonatation of the mineral phase

We then explored the mineral phase composition and structure of the HELIX dental tissues by Raman microscopy. Control and HELIX enamel samples were analyzed by recording Raman mappings based on the FWHM of the $\nu(PO_4^{3-})$ band (Figure 3), indicative of the crystallinity of the apatite component of the tooth, and on the ratio between the integrated area of the $\nu(CO_3^{2-})$ and $\nu(PO_4^{3-})$ vibration bands, indicative of the carbonatation rate of this apatite component.[58] The selected area extended from the outer enamel layer to the dentin core (Figure 3A,D). For the control sample, largest $FHWM_{960}$ were found in the dentin area and, after an intermediate layer, the enamel part was characterized by a quite homogeneous, smaller $FHWM_{960}$ value (Figure 3B). Similarly, the I_{1070}/I_{960} ratio decreased from dentin to enamel but the area with intermediate values extended much significantly in the latter tissue (Figure 3C). These results are consistent with the fact that
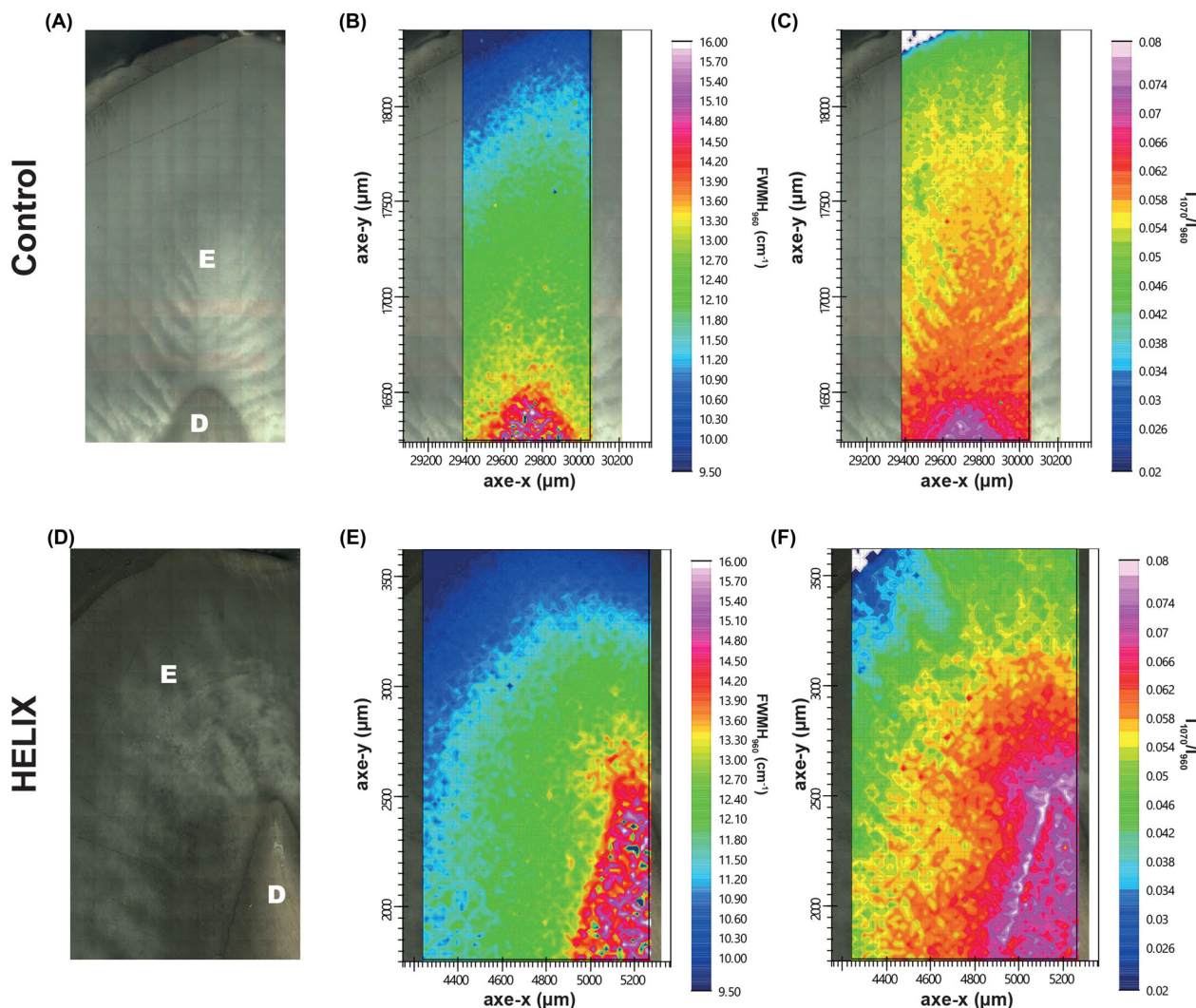
FIGURE 3 Characterization of the HELIX tooth using Raman microspectroscopy. (A,D) Optical microscopy of the imaged section of control and HELIX samples. (B,E) Raman mapping of the control and HELIX samples based on the full width at half maxima (FWHM) of the $\nu(PO_4^{3-})$ vibration band at 960 cm^{-1}. (C,F) Raman mapping of control and HELIX samples based on the ratio between the integrated area of the $\nu(CO_3^{2-})$ and $\nu(PO_4^{3-})$ vibration bands at 1070 and 960 cm^{-1}, respectively. Abbreviations: D, dentin; E, enamel.

the mineral phase of enamel is a highly crystalline hydroxyapatite with low carbonatation rate, whereas the mineral phase of dentin has a higher degree of substitution and lower crystallinity.[59] No significant difference in the evolution of both FHWM$_{960}$ (Figure 3E) and I$_{1070}$/I$_{960}$ (Figure 3F) values from dentin to enamel could be evidenced in the HELIX sample compared to the control, suggesting the absence of modification of the crystallinity and carbonatation degree of the mineral phase in these two tissues.

Chemical analyses

An investigation on the chemical composition of the enamel was performed to determine if it was altered, which would indicate an abnormal maturation and contribute to explaining the rapid enamel wear observed in all the patients with the HELIX syndrome.[34] EDX analysis revealed that the Ca/P ratio was slightly lower in the HELIX enamel, especially in the outer layer, when compared to the control

enamel (outer enamel layer: 1.54 vs. 1.58; inner layer: 1.59 vs. 1.60, respectively), and this was mainly due to a slightly lower Ca content (Table 1; Figures S2 and S3). As most of the patients with HELIX syndrome have been reported to have hypermagnesemia,[32,34] the (Ca + Mg)/P ratio was also calculated, revealing a similar pattern in both enamel samples (Table 1). No differences were found for the dentin by either SEM (Figure S4) or EDX (data not shown).

Next, multielement analysis of the samples was performed using SXRF to investigate further possible modifications of the chemical composition of enamel induced by the HELIX syndrome (Figure 4).

Calcium

In the HELIX tooth, the SXRF levels of Ca in enamel and dentin are uniform and reach on average 4.0×10^5 ppm and 3.4×10^5 ppm, respectively (Figure 4, left upper panel). In the control tooth (permanent third molar), Ca levels range between 3.6×10^5 and
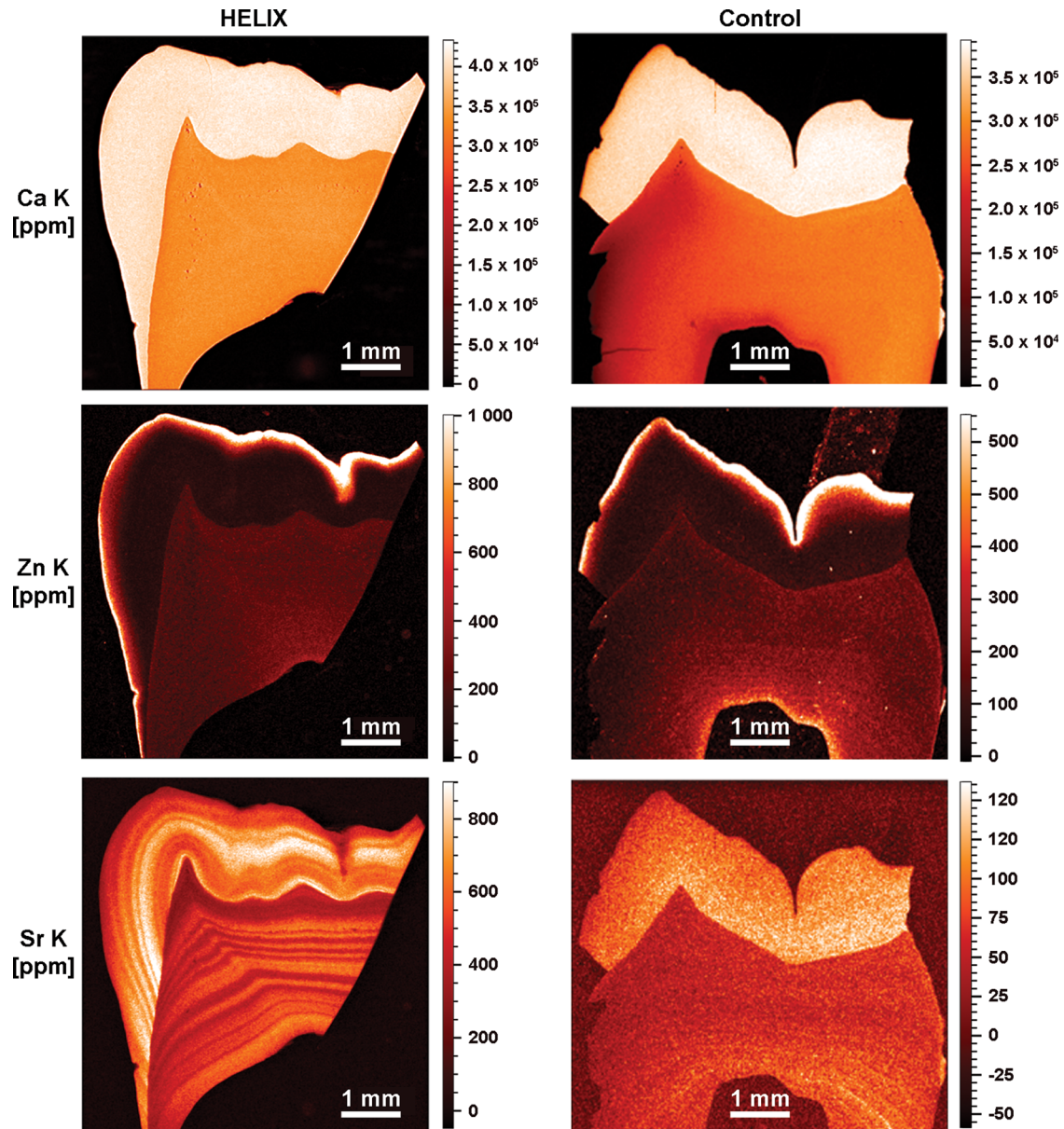
FIGURE 4 SXRF characterization of the HELIX molar. SXRF characterization of the HELIX (left) and control (right) teeth for mapping Ca (upper panel), Zn (middle panel), and Sr (lower panel) (SXRF overviews at 10 μm). In both the HELIX and control molar crowns, Ca and Zn have a similar distribution with comparable ranges of concentration (in ppm). HELIX shows Sr levels that are six times higher than in the control, with marked patterns of alternating Sr enrichments and depletions in both the enamel and the dentin.

3.85×10^5 ppm in enamel, and between 2.0×10^5 and 2.8×10^5 ppm in dentin (Figure 4, right upper panel). These Ca values are compatible with the published values of enamel and dentin imaged by SXRF, ranging from 3.8×10^5 to 5.0×10^5 and from 3.1×10^5 to 3.7×10^5 ppm, respectively.[60–63] The present results show that *CLDN10* deficiency did not alter significantly the process of tooth tissue mineralization.

Zinc

Zn levels imaged by SXRF in the first-formed inner enamel are relatively low. They rise in a steep gradient toward the OES, where Zn levels are greatly enriched. In HELIX tooth, the OES at the occlusal basin reaches 1.8×10^3 ppm, while at the lateral enamel surface, it peaks at 1.2×10^3 ppm (Figure 4, left middle panel). The middle and inner enamel is at ~100 ppm, while the dentin is at ~220 ppm. In the control sample, although the enamel cap is not fully preserved, Zn values at the OES peak at $\sim 1.0 \times 10^3$ ppm on the occlusal aspect of the cusps, while it is slightly less on the surface of the lateral enamel (600–800 ppm). The inner and middle zones of enamel contain ~60 to ~100 ppm of Zn, while the dentin is at ~200 ppm. Zinc enrichment at the OES has been previously described as a normal feature, potentially related to the processes of enamel mineralization and maturation.[60,64,65] SXRF values in human deciduous teeth show peak

TABLE 1 Atomic quantification of elements (in At [%]) in HELIX and control in the inner and outer layers of enamel by EDX analyses

Element	HELIX			Control		
	P	Ca	Mg	P	Ca	Mg
Outer						
Max	13.7	21.0	0.2	13.7	21.6	0.2
Min	13.5	20.9	0.1	13.5	21.4	0.1
Average	13.6	21.0	0.2	13.6	21.5	0.2
Standard deviation	0.1	0.1	0.0	0.1	0.1	0.0
Ca/P		1.54			1.58	
(Ca+Mg)/P		1.55			1.59	
Inner						
Max	13.6	21.4	0.5	14.0	22.4	0.4
Min	12.7	20.2	0.4	13.8	22.1	0.4
Average	13.0	20.7	0.4	13.9	22.2	0.4
Standard deviation	0.5	0.7	0.1	0.1	0.2	0.0
Ca/P		1.59			1.60	
(Ca+Mg)/P		1.62			1.62	

values ranging from 400 to 500 ppm at the OES,[60] while in *Pongo*, the outer layer of enamel concentrates 1.5×10^3 to 2.0×10^3 ppm of Zn.[66] Rautray *et al.*[67] reported Zn values on human healthy enamel yielding an average of 172.2 ppm, which is within the same order of magnitude as the present middle and inner values measured in HELIX and control.

Strontium

In the control tooth, the Sr distribution (Figure 4, right lower panel) followed previously published observations.[60] On average, Sr levels in enamel ranged from 50 to 130 ppm (outer vs. inner enamel, respectively), which is compatible with an average of 174.76 ppm calculated from values provided in Ref. 67. In dentin, Sr values in the control tooth ranged between 40 and 80 ppm, with an accentuated event at 150 ppm. In the HELIX sample (Figure 4, left lower panel), a strong pattern of variation in Sr concentrations was visible using SXRF in both the enamel and dentin, from the earliest stages of formation of the third molar until crown completion and beyond into the root dentin. An alternation of strong depletions and enrichments occurred with a high frequency. Both HR SXRF scans at 1.5 μm confirmed that these accentuated Sr markings occurred simultaneously in enamel and dentin (Figure S5). As the abrupt changes in the content of Sr followed the direction of the striae of Retzius (Figure 5A), further investigation was performed to determine whether these events take place at specific periods during the crown formation, with no overprinting from subsequent Sr ingestions.[66] Within the ~1330 μm of cuspal enamel, these several episodes of Sr variation were each calculated to last from 33 to 121 days, (Figure 5B and Table S2). Within enamel, these bands of Sr variations peaked at 860 ppm (direct measurement in HDIP v-1.3.3.1073, outside of the blue transect in Figure 5A) in the

middle of the cuspal enamel, while the strongest depletions dropped down to ~300–350 ppm, especially at the OES (Figure 4, left lower panel). In dentin, values were lower with peaks at 600–650 ppm and troughed at 280–340 ppm (Figure 4, left lower panel). The variation in Sr concentration as well as their timing in days did not suggest that these changes followed any regular and periodical pattern. These findings prompted us to question the HELIX patient on a particular exposure to strontium at any time of her growth, including the period corresponding to the third molar formation. She did not report either a specific diet or using any specific toothpaste enriched in strontium ions to prevent tooth hypersensitivity.

Other elements

Other elements with Kα lines in the detectable energy range, which include Cu, Fe, Mn, Ti, Cr, S, Cl, Ar, and Rb, did not yield any significant detectable differences between the HELIX and the control tooth in terms of elemental distribution or abundance (Figure S6).

DISCUSSION

The HELIX syndrome is a very rare disorder (OMIM 617671; Prevalence: <1/1,000,000), which manifests as abnormalities in renal ion homeostasis, resulting in hypermagnesemia, hypocalciuria, and hypokalemia, in epidermal integrity and homeostasis of the ectodermal glands, including salivary glands. We previously reported that all patients with HELIX syndrome displayed early and severe enamel wear,[34] compromising their oral health and particularly their chewing capacity. The present study is based on the observation of a third molar from a patient with HELIX syndrome, which was collected prior to the full eruption of the tooth and, therefore, before the crown was fully exposed to the challenges of the environment of the oral cavity,[68–70] and shows that the enamel was correctly formed and displayed normal maturation.

The general pattern of enamel formation appears to be consistent with that described for normal human permanent molars.[54] Specifically, the DSR gradient increase from the EDJ to the surface in the cuspal enamel matches that in normal third permanent molars. The time taken to form lateral enamel is also within the ranges reported for human third permanent molars,[42] and the total enamel formation time is within the ranges reported in the literature.[42,52,71,72] It seems unlikely, therefore, that the HELIX syndrome has any impact on the timing of enamel formation.

The structure of enamel in both HELIX and control samples was studied both at the microscale by SEM and Raman spectroscopy. Although these techniques were previously shown to clearly characterize other dental disorders, such as *Amelogenesis imperfecta*[73,74] or X-linked hypophosphatemia,[75] no significant difference could be found in the present study between the HELIX and the control molars.

Similarly, the EDX determination of the Ca, P, and Mg content led to similar values for both samples. However, this technique has a rather
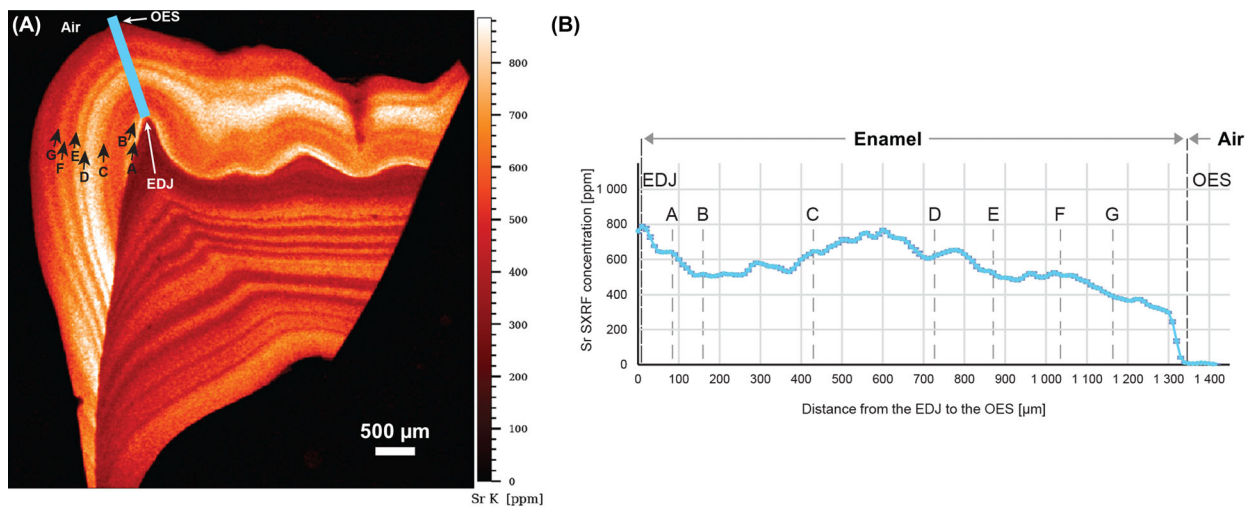
FIGURE 5 Variations in Sr content in the cuspal enamel of the HELIX tooth. (A) Sr SXRF map of the HELIX tooth showing the variation in Sr content in enamel and dentin. Datapoints were collected along the blue transect to plot Sr concentrations as a function of distance (see B) from the enamel–dentin junction (EDJ) to the outer enamel surface (OES). Marked Sr variations following the direction of the enamel growth lines were attributed letters (from A to H; black arrows). There is no clear temporal periodicity in the occurrence of these Sr variations.

high detection limit (~1000 ppm), especially for light elements. In contrast, SXRF allows for quantification below 1 ppm and was already applied for multielement analysis of trace elements in many biological tissues,[76] including teeth.[60,66] Here, among the many collected elements, Sr stood out as the only investigated element showing a clear difference in amount and distribution between the two samples. Not only its local concentration could be six times higher in the enamel of the HELIX tooth compared to the control, but it also formed well-defined zones of enrichment and depletion parallel to the striae of Retzius, attesting that this chemical signal has been integrated to the dental tissues during development. However, in contrast to these periodical growth markings, no periodicity could be found in the occurrence of these Sr bands, suggesting that Sr incorporation is not linked to a specific, regular step of amelogenesis. In fact, it is notable that Sr bands are also present synchronously in the dentin, suggesting that Sr presence is related to an overall mineral homeostasis disorder rather than to a local disturbance of amelogenesis.

Dental hard tissues contain trace elements of both dietary and environmental origin.[77] Among them, strontium ions are divalent cations and thus can easily substitute for Ca in the hydroxyapatite structure or interact with the mineral phase.[78] It has been previously reported that the substitution of Ca by Sr in hydroxyapatite alters its solubility.[79] However, this was demonstrated for Sr amount above 1%,[79] which is not the case in the present tooth analysis, where the substitution appears to occur at 0.1%. Therefore, although we cannot fully exclude a modification of apatite solubility with such a low substitution rate, it is expected to be very minor. In vivo, it was found that by oral treatment of increasing Sr dose in rats, it was possible to obtain Sr/(Sr + Ca) molar ratio > 0.01 in femur without altering the bone structure.[80] As a comparison, the Sr/(Sr + Ca) molar ratio here was ~0.002, which could explain the absence of a clear difference in the enamel structure between HELIX and control in this study. Accordingly, it was not possi-

ble to detect Sr-related spatial variations of Ca amount in the Ca SXRF map. A possible explanation of this high and random adsorption of Sr within enamel and dentin might be an excess of strontium consumption in the patient's diet or by swallowing toothpaste.[81] However, our HELIX patient, who was born and raised in France, did not report either a specific diet or using, at any time of her growth, including the period corresponding to the third molar formation, any specific toothpaste enriched in strontium ions to prevent tooth hypersensitivity.

The renal clearance of Sr can be computed to 2–3 ml/min in normal subjects. It is much lower than normal glomerular filtration rate, indicating that Sr excreted in urine is only a tiny fraction of filtered Sr: therefore, most of Sr filtered at the glomerulus is reabsorbed along the renal tubule, as Ca and Mg are.[82,83] Patients with HELIX syndrome have very low urinary calcium and magnesium excretion in urine, despite normal serum Ca and high serum Mg levels, indicative of increased tubular Ca and Mg reabsorption.[32] That Sr is also excessively reabsorbed across the renal tubular epithelium is a sound hypothesis, albeit not documented. Subsequently, patients with HELIX syndrome may have a higher than normal serum Sr concentration, all the more so since serum Sr level increases when GFR decreases.[82] Thus, a higher serum Sr level may result in a higher deposition of Sr in bone and tooth. Future studies are needed to investigate whether abnormal levels of Sr are also identified in bones of HELIX syndrome patients and, more broadly, how the kidney dysfunction associated with the HELIX syndrome impacts plasma and urine Sr concentrations.

One of the main functions of the enamel organ during the maturation stage is to transport very large amounts of mineral ions, especially calcium and phosphate, from the blood vessels to the enamel matrix. This critical process is finely controlled by a great number of ion channels, transporters, and exchangers.[10,11,84,85] In the HELIX syndrome, one of the consequences of the renal dysfunction is hypocalciuria.[32]

The precise role of Mg in amelogenesis remains not fully understood, yet the expression of the Mg transporter CNNM4 in ameloblast cell membranes at the transition and maturation stages supports that Mg might be removed from the enamel matrix to promote mineralization.[86] It has indeed been consistently reported that Mg content of the enamel is inversely correlated with the extent of mineralization.[87,88] Here, the magnesium content was found to be normal in the HELIX enamel, suggesting that the hypermagnesemia found in the HELIX patients[32] may not have direct consequence on enamel mineralization.

Hypokalemia is a frequent feature of the HELIX patients.[32] Potassium ions have been shown to be important for normal enamel formation as several ion exchangers or cotransporters are K^+-dependent.[10,11,84,89] For example, the alteration of the K^+-dependent Na^+/Ca^{2+} exchanger isoform 4 (*SLC24A4*) into mouse maturation ameloblasts by an excess of fluoride in the drinking water was shown to impair amelogenesis.[89] Furthermore, patients with syndromes associated with hypokalemia, such as the Bartter's syndrome, were reported to display *Amelogenesis imperfecta*.[90,91] It is, therefore, likely that the hypokalemia measured in the patients with the HELIX syndrome may contribute to higher enamel fragility.

Taken together, our data show that enamel formation is not significantly impaired by *CLDN10* deficiency, rather designating xerostomia as the main culprit of the enamel wear found in HELIX patients. However, the abnormal concentrations of Sr measured in the dental mineralized tissues suggest that the tooth mineral content may reflect repeated episodes of worsening of renal dysfunction. It cannot be denied that such changes in Sr concentrations, albeit very low, may alter enamel and dentin solubility. These events urge the need to investigate more teeth from HELIX patients. Serum strontium concentration should also be monitored. Nevertheless, the study of a murine model of the HELIX syndrome may provide further insights on the direct role of claudin-10 in amelogenesis.

AUTHOR CONTRIBUTIONS

C.C., F.R.R., T.C., and T.B. conceived and designed the study. F.R.R., N.O., T.N.N., and E.G. prepared the tooth thin-sections. J.G., A.L.C., M.C.D., and S.J.M.V.M. acquired the SXRF data. S.J.M.V.M. and J.G. postprocessed the SXRF data. A.P. and C.P. recorded the Raman data. A.P., C.P., and T.C. interpreted the Raman data. C.C., N.O., and T.C. interpreted the SEM and EDX data. A.L.C., F.R.R., and M.C.D. analyzed and interpreted the SXRF data. C.C., N.O., A.L.C., C.B., T.C., P.H., S.H.R., and F.R.R. drafted the manuscript, and with revisions and final approval of the submitted version by all coauthors.

COMPETING INTERESTS

The authors declare no competing interests.

PEER REVIEW

The peer review history for this article is available at: https://publons.com/publon/10.1111/nyas.14865.

ORCID

Nicolas Obtel https://orcid.org/0000-0001-5117-6944
Adeline Le Cabec https://orcid.org/0000-0001-6948-4726
Eloise Giabicani https://orcid.org/0000-0001-8122-760X
Stijn J. M. Van Malderen https://orcid.org/0000-0002-3879-7882
Jan Garrevoet https://orcid.org/0000-0001-8696-0499
Aline Percot https://orcid.org/0000-0002-3896-314X
Christopher Dean https://orcid.org/0000-0003-3783-7296
Smail Hadj-Rabia https://orcid.org/0000-0001-6801-7106
Pascal Houillier https://orcid.org/0000-0003-4953-6917
Claire Bardet https://orcid.org/0000-0002-0874-4843
Thibaud Coradin https://orcid.org/0000-0003-3374-5722
Fernando Ramirez Rozzi https://orcid.org/0000-0002-8537-3839
Catherine Chaussain https://orcid.org/0000-0002-3463-3936

REFERENCES

1. Thesleff, I. (2003). Epithelial–mesenchymal signalling regulating tooth morphogenesis. *Journal of Cell Science*, 116, 1647–1648.
2. Catón, J., & Tucker, A. S. (2009). Current knowledge of tooth development: Patterning and mineralization of the murine dentition. *Journal of Anatomy*, 214, 502–515.
3. Balic, A., & Thesleff, I. (2015). Tissue interactions regulating tooth development and renewal. *Current Topics in Developmental Biology*, 115, 157–186.
4. Kovacs, C. S., Chaussain, C., Osdoby, P., Brandi, M. L., Clarke, B., & Thakker, R. V. (2021). The role of biomineralization in disorders of skeletal development and tooth formation. *Nature Reviews Endocrinology*, 17, 336–349.
5. Hu, J. C.-C., Chun, Y.-H. P., Al Hazzazzi, T., & Simmer, J. P. (2007). Enamel formation and *Amelogenesis imperfecta*. *Cells, Tissues, Organs*, 186, 78–85.
6. Lacruz, R. S., Habelitz, S., Wright, J. T., & Paine, M. L. (2017). Dental enamel formation and implications for oral health and disease. *Physiological Reviews*, 97, 939–993.
7. Moradian-Oldak, J., & George, A. (2021). Biomineralization of enamel and dentin mediated by matrix proteins. *Journal of Dental Research*, 100, 1020–1029.

8. Habelitz, S., & Bai, Y. (2021). Mechanisms of enamel mineralization guided by amelogenin nanoribbons. *Journal of Dental Research*, *100*, 1434–1443.

9. Smith, C. E. (1998). Cellular and chemical events during enamel maturation. *Critical Reviews in Oral Biology and Medicine*, *9*, 128–161.

10. Bronckers, A. L. J. J. (2017). Ion transport by ameloblasts during amelogenesis. *Journal of Dental Research*, *96*, 243–253.

11. Lacruz, R. S., Smith, C. E., Kurtz, I., Hubbard, M. J., & Paine, M. L. (2013). New paradigms on the transport functions of maturation-stage ameloblasts. *Journal of Dental Research*, *92*, 122–129.

12. Lacruz, R. S., Smith, C. E., Moffatt, P., Chang, E. H., Bromage, T. G., Bringas, P., Nanci, A., Baniwal, S. K., Zabner, J., Welsh, M. J., Kurtz, I., & Paine, M. L. (2012). Requirements for ion and solute transport, and pH regulation during enamel maturation. *Journal of Cellular Physiology*, *227*, 1776–1785.

13. Bartlett, J. D., & Smith, C. E. (2013). Modulation of cell–cell junctional complexes by matrix metalloproteinases. *Journal of Dental Research*, *92*, 10–17.

14. Günzel, D., & Yu, A. S. L. (2013). Claudins and the modulation of tight junction permeability. *Physiological Reviews*, *93*, 525–569.

15. Hata, M., Kawamoto, T., Kawai, M., & Yamamoto, T. (2010). Differential expression patterns of the tight junction-associated proteins occludin and claudins in secretory and mature ameloblasts in mouse incisor. *Medical Molecular Morphology*, *43*, 102–106.

16. Bardet, C., Courson, F., Wu, Y., Khaddam, M., Salmon, B., Ribes, S., Thumfart, J., Yamaguti, P. M., Rochefort, G. Y., Figueres, M.-L., Breiderhoff, T., Garcia-Castaño, A., Vallée, B., Le Denmat, D., Baroukh, B., Guilbert, T., Schmitt, A., Massé, J.-M., Bazin, D., … Chaussain, C. (2016). Claudin-16 deficiency impairs tight junction function in ameloblasts, leading to abnormal enamel formation. *Journal of Bone and Mineral Research*, *31*, 498–513.

17. Bardet, C., Ribes, S., Wu, Y., Diallo, M. T., Salmon, B., Breiderhoff, T., Houillier, P., Müller, D., & Chaussain, C. (2017). Claudin loss-of-function disrupts tight junctions and impairs amelogenesis. *Frontiers in Physiology*, *8*, 326.

18. Yamaguti, P. M., Neves, F. D. A. R., Hotton, D., Bardet, C., De La Dure-Molla, M., Castro, L. C., Scher, M. D. C., Barbosa, M. E., Ditsch, C., Fricain, J.-C., De La Faille, R., Figueres, M.-L., Vargas-Poussou, R., Houiller, P., Chaussain, C., Babajko, S., Berdal, A., & Acevedo, A. C. (2017). *Amelogenesis imperfecta* in familial hypomagnesaemia and hypercalciuria with nephrocalcinosis caused by CLDN19 gene mutations. *Journal of Medical Genetics*, *54*, 26–37.

19. Wang, X., Chiba, Y., Jia, L., Yoshizaki, K., Saito, K., Yamada, A., Qin, M., & Fukumoto, S. (2020). Expression patterns of claudin family members during tooth development and the role of claudin-10 (Cldn10) in cytodifferentiation of stratum intermedium. *Frontiers in Cell and Developmental Biology*, *8*, 595593.

20. Van Itallie, C. M., & Anderson, J M. (2006). Claudins and epithelial paracellular transport. *Annual Review of Physiology*, *68*, 403–429.

21. Prot-Bertoye, C., Griveau, C., Skjødt, K., Cheval, L., Brideau, G., Lievre, L., Ferriere, E., Arbaretaz, F., Garbin, K., Zamani, R., Marcussen, N., Figueres, L., Breiderhoff, T., Muller, D., Bruneval, P., Houillier, P., & Dimke, H. (2021). Differential localization patterns of claudin 10, 16, and 19 in human, mouse, and rat renal tubular epithelia. *American Journal of Physiology-Renal Physiology*, *321*, F207–F224.

22. Milatz, S., & Breiderhoff, T. (2017). One gene, two paracellular ion channels—Claudin-10 in the kidney. *Pflugers Archiv: European Journal of Physiology*, *469*, 115–121.

23. Breiderhoff, T., Himmerkus, N., Stuiver, M., Mutig, K., Will, C., Meij, I. C., Bachmann, S., Bleich, M., Willnow, T. E., & Müller, D. (2012). Deletion of claudin-10 (Cldn10) in the thick ascending limb impairs paracellular sodium permeability and leads to hypermagnesemia and nephrocalcinosis. *Proceedings of the National Academy of Sciences of the United States of America*, *109*, 14241–14246.

24. Günzel, D., Stuiver, M., Kausalya, P. J, Haisch, L., Krug, S. M., Rosenthal, R., Meij, I. C., Hunziker, W., Fromm, M., & Müller, D. (2009). Claudin-10 exists in six alternatively spliced isoforms that exhibit distinct localization and function. *Journal of Cell Science*, *122*, 1507–1517.

25. Inai, T., Sengoku, A., Guan, X., Hirose, E., Iida, H., & Shibata, Y. (2005). Heterogeneity in expression and subcellular localization of tight junction proteins, claudin-10 and -15, examined by RT-PCR and immunofluorescence microscopy. *Archives of Histology and Cytology*, *68*, 349–360.

26. Smith, C. E. L., Poulter, J. A., Antanaviciute, A., Kirkham, J., Brookes, S. J., Inglehearn, C. F., & Mighell, A. J. (2017). *Amelogenesis imperfecta*; Genes, proteins, and pathways. *Frontiers in Physiology*, *8*, 435.

27. Chen, C.-F., Hu, J. C., Bresciani, E., Peters, M. C., & Estrella, M. R. P. (2013). Treatment considerations for patient with *Amelogenesis imperfecta*: A review. *Brazilian Dental Science*, *16*, 7–18.

28. Dashash, M., Yeung, C. A., Jamous, I., & Blinkhorn, A. (2013). Interventions for the restorative care of *Amelogenesis imperfecta* in children and adolescents. *Cochrane Database of Systematic Reviews*, *2013*, CD007157.

29. Friedlander, L., Berdal, A., Boizeau, P., Licht, B. A., Manière, M.-C., Picard, A., Azzis, O., Vazquez, M.-P., Alberti, C., & Molla, M. D. L. D. (2019). Oral health related quality of life of children and adolescents affected by rare orofacial diseases: A questionnaire-based cohort study. *Orphanet Journal of Rare Diseases*, *14*, 124.

30. de La Dure-Molla, M., Fournier, B. P., Manzanares, M. C., Acevedo, A. C., Hennekam, R. C., Friedlander, L., Boy-Lefèvre, M.-L., Kerner, S., Toupenay, S., Garrec, P., Vi-fane, B., Felizardo, R., Berteretche, M.-V., Jordan, L., Ferré, F., Clauss, F., Jung, S., Chalendar, M., Troester, S., … Bloch-Zupan, A. (2019). Elements of morphology: Standard terminology for the teeth and classifying genetic dental disorders. *American Journal of Medical Genetics-Part A*, *179*, 1913–1981.

31. Crawford, P. J., Aldred, M., & Bloch-Zupan, A. (2007). Amelogenesis imperfecta. *Orphanet Journal of Rare Diseases*, *2*, 17.

32. Milatz, S. (2019). A novel claudinopathy based on claudin-10 mutations. *International Journal of Molecular Sciences*, *20*, 5396.

33. Klar, J., Piontek, J., Milatz, S., Tariq, M., Jameel, M., Breiderhoff, T., Schuster, J., Fatima, A., Asif, M., Sher, M., Mäbert, K., Fromm, A., Baig, S. M., Günzel, D., & Dahl, N. (2017). Altered paracellular cation permeability due to a rare CLDN10B variant causes anhidrosis and kidney damage. *PLoS Genetics*, *13*, e1006897.

34. Hadj-Rabia, S., Brideau, G., Al-Sarraj, Y., Maroun, R. C., Figueres, M.-L., Leclerc-Mercier, S., Olinger, E., Baron, S., Chaussain, C., Nochy, D., Taha, R. Z., Knebelmann, B., Joshi, V., Curmi, P. A., Kambouris, M., Vargas-Poussou, R., Bodemer, C., Devuyst, O., Houillier, P., & El-Shanti, H. (2018). Multiplex epithelium dysfunction due to CLDN10 mutation: The HELIX syndrome. *Genetics in Medicine*, *20*, 190–201.

35. Vargas-Poussou, R. (2021). Pathophysiological aspects of the thick ascending limb and novel genetic defects: HELIX syndrome and transient antenatal Bartter syndrome. *Pediatric Nephrology*, *37*, 239–252.

36. Alzahrani, A. S., Hussein, M., Alswailem, M., Mouna, A., Albalawi, L., Moria, Y., Jabbar, M. A., Shi, Y., Günzel, D., & Dasouki, M. (2021). A novel claudin-10 mutation with a unique mechanism in two unrelated families with HELIX syndrome. *Kidney International*, *100*, 415–429.

37. Bongers, E. M. H. F., Shelton, L. M., Milatz, S., Verkaart, S., Bech, A. P., Schoots, J., Cornelissen, E. A. M., Bleich, M., Hoenderop, J. G. J., Wetzels, J. F. M., Lugtenberg, D., & Nijenhuis, T. (2017). A novel hypokalemic-alkalotic salt-losing tubulopathy in patients with CLDN10 mutations. *Journal of the American Society of Nephrology*, *28*, 3118–3128.

38. Lacruz, R. S., Hacia, J. G., Bromage, T. G., Boyde, A., Lei, Y., Xu, Y., Miller, J. D., Paine, M. L., & Snead, M. L. (2012). The circadian clock modulates enamel development. *Journal of Biological Rhythms*, *27*, 237–245.

39. Ramirez Rozzi, F. (1998). Enamel structure and development and its application in hominid evolution and taxonomy. *Journal of Human Evolution*, *35*, 327–330.

40. Dean, M. C. (1998). A comparative study of cross striation spacings in cuspal enamel and of four methods of estimating the time taken to grow molar cuspal enamel in Pan, Pongo and Homo. *Journal of Human Evolution*, *35*, 449–462.

41. Beynon, A. D, Dean, M. C, Leakey, M. G, Reid, D. J, & Walker, A. (1998). Comparative dental development and microstructure of Proconsul teeth from Rusinga Island, Kenya. *Journal of Human Evolution*, *35*, 163–209.

42. Reid, D. J., & Dean, M. C. (2006). Variation in modern human enamel formation times. *Journal of Human Evolution*, *50*, 329–346.

43. Timchenko, P. E., Timchenko, E. V., Pisareva, E. V., Vlasov, M. Yu., Volova, L. T., Frolov, O. O., & Kalimullina, A. R. (2018). Experimental studies of hydroxyapatite by Raman spectroscopy. *Journal of Optical Technology*, *85*, 130–135.

44. Boesenberg, U., Ryan, C. G., Kirkham, R., Siddons, D. P., Alfeld, M., Garrevoet, J., Núñez, T., Claussen, T., Kracht, T., & Falkenberg, G. (2016). Fast X-ray microfluorescence imaging with submicrometer-resolution integrating a Maia detector at beamline P06 at PETRA III. *Journal of Synchrotron Radiation*, *23*, 1550–1560.

45. Schroer, C. G., Boye, P., Feldkamp, J. M., Patommel, J., Samberg, D., Schropp, A., Schwab, A., Stephan, S., Falkenberg, G., Wellenreuther, G., & Reimers, N. (2010). Hard X-ray nanoprobe at beamline P06 at PETRA III. *Nuclear Instruments and Methods in Physics Research Section A*, *616*, 93–97.

46. Falkenberg, G., Fleissner, G., Fleissner, G., Alraun, P., Boesenberg, U., & Spiers, K. (2017). Large-scale high-resolution micro-XRF analysis of histological structures in the skin of the pigeon beak. *X-Ray Spectrometry*, *46*, 467–473.

47. Solé, V. A., Papillon, E., Cotte, M., Walter, Ph., & Susini, J. (2007). A multiplatform code for the analysis of energy-dispersive X-ray fluorescence spectra. *Spectrochimica Acta B*, *62*, 63–68.

48. Djomehri, S. I., Candell, S., Case, T., Browning, A., Marshall, G. W., Yun, W., Lau, S. H., Webb, S., & Ho, S. P. (2015). Mineral density volume gradients in normal and diseased human tissues. *PLoS One*, *10*, e0121611.

49. Szczerbowska-Boruchowska, M. (2012). Sample thickness considerations for quantitative X-ray fluorescence analysis of the soft and skeletal tissues of the human body — Theoretical evaluation and experimental validation. *X-Ray Spectrometry*, *41*, 328–337.

50. Schneider, C. A., Rasband, W. S., & Eliceiri, K. W. (2012). NIH Image to ImageJ: 25 years of image analysis. *Nature Methods*, *9*, 671–675.

51. Schindelin, J., Arganda-Carreras, I., Frise, E., Kaynig, V., Longair, M., Pietzsch, T., Preibisch, S., Rueden, C., Saalfeld, S., Schmid, B., Tinevez, J.-Y., White, D. J., Hartenstein, V., Eliceiri, K., Tomancak, P., & Cardona, A. (2012). Fiji: An open-source platform for biological-image analysis. *Nature Methods*, *9*, 676–682.

52. Dean, C., Zanolli, C., Le Cabec, A., Tawane, M., Garrevoet, J., Mazurier, A., & Macchiarelli, R. (2020). Growth and development of the third permanent molar in *Paranthropus robustus* from Swartkrans, South Africa. *Scientific Reports*, *10*, 19053.

53. Smith, T. M., Olejniczak, A. J., Reid, D. J., Ferrell, R. J., & Hublin, J. J. (2006). Modern human molar enamel thickness and enamel–dentine junction shape. *Archives of Oral Biology*, *51*, 974–995.

54. Mahoney, P. (2008). Intraspecific variation in M1 enamel development in modern humans: Implications for human evolution. *Journal of Human Evolution*, *55*, 131–147.

55. Lacruz, R. S., Dean, M. C., Ramirez-Rozzi, F., & Bromage, T. G. (2008). Megadontia, striae periodicity and patterns of enamel secretion in Plio-Pleistocene fossil hominins. *Journal of Anatomy*, *213*, 148–158.

56. Lacruz, R. S., & Bromage, T. G. (2006). Appositional enamel growth in molars of South African fossil hominids. *Journal of Anatomy*, *209*, 13–20.

57. Li, C., & Risnes, S. (2004). SEM observations of Retzius lines and prism cross-striations in human dental enamel after different acid etching regimes. *Archives of Oral Biology*, *49*, 45–52.

58. Bērziņš, K., Sutton, J. J., Loch, C., Beckett, D., Wheeler, B. J., Drummond, B. K., Fraser-Miller, S. J., & Gordon, K. C. (2019). Application of low-wavenumber Raman spectroscopy to the analysis of human teeth. *Journal of Raman Spectroscopy*, *50*, 1375–1387.

59. Ortiz-Ruiz, A. J., Teruel-Fernández, J. D. D., Alcolea-Rubio, L. A., Hernández-Fernández, A., Martínez-Beneyto, Y., & Gispert-Guirado, F. (2018). Structural differences in enamel and dentin in human, bovine, porcine, and ovine teeth. *Annals of Anatomy*, *218*, 7–17.

60. Dean, M. C., Spiers, K. M., Garrevoet, J., & Le Cabec, A. (2019). Synchrotron X-ray fluorescence mapping of Ca, Sr and Zn at the neonatal line in human deciduous teeth reflects changing perinatal physiology. *Archives of Oral Biology*, *104*, 90–102.

61. Rautray, T. R., Das, S., & Rautray, A. C. (2010). In situ analysis of human teeth by external PIXE. *Nuclear Instruments and Methods in Physics Research Section B*, *268*, 2371–2374.

62. Daculsi, G., Bouler, J. M., & LeGeros, R. Z. (1997). Adaptive crystal formation in normal and pathological calcifications in synthetic calcium phosphate and related biomaterials. *International Review of Cytology*, *172*, 129–191.

63. Lane, D. W., & Peach, D. F. (1997). Some observations on the trace element concentrations in human dental enamel. *Biological Trace Element Research*, *60*, 1–11.

64. Humphrey, L. T., Dean, M. C., Jeffries, T. E., & Penn, M. (2008). Unlocking evidence of early diet from tooth enamel. *Proceedings of the National Academy of Sciences of the United States of America*, *105*, 6834–6839. PMID: 18458343.

65. Müller, W., Nava, A., Evans, D., Rossi, P. F., Alt, K. W., & Bondioli, L. (2019). Enamel mineralization and compositional time-resolution in human teeth evaluated via histologically-defined LA-ICPMS profiles. *Geochimica et Cosmochimica Acta*, *255*, 105–126.

66. Dean, M. C., Le Cabec, A., Van Malderen, S. J. M., & Garrevoet, J. (2020). Synchrotron X-ray fluorescence imaging of strontium incorporated into the enamel and dentine of wild-shot orangutan canine teeth. *Archives of Oral Biology*, *119*, 104879.

67. Rautray, T. R., Dutta, K., Das, S. L., & Rautray, A. C. (2010). In situ analyses of gallstone inner layers by external PIXE. *Nuclear Instruments and Methods in Physics Research Section B*, *268*, 2773–2776.

68. Lamster, I. B., Asadourian, L., Del Carmen, T., & Friedman, P. K. (2016). The aging mouth: Differentiating normal aging from disease. *Periodontology*, *72*, 96–107.

69. Hara, A. T., Lussi, A., & Zero, D. T. (2006). Biological factors. *Monographs in Oral Science*, *20*, 88–99.

70. Buzalaf, M.-L. A. R., Hannas, A. R., & Kato, M. T. (2012). Saliva and dental erosion. *Journal of Applied Oral Science*, *20*, 493–502.

71. Dean, M. C. (2010). Retrieving chronological age from dental remains of early fossil hominins to reconstruct human growth in the past. *Philosophical Transactions of the Royal Society of London. Series B, Biological Sciences*, *365*, 3397–3410.

72. Anemone, R. L., Mooney, M. P., & Siegel, M. I. (1996). Longitudinal study of dental development in chimpanzees of known chronological age: Implications for understanding the age at death of Plio-Pleistocene hominids. *American Journal of Physical Anthropology*, *99*, 119–133.

73. Wang, P., Anderson, E. J. D., Muller, E. A., Gao, F., Zhong, Y., & Raschke, M. B. (2018). Hyper-spectral Raman imaging correlating chemical substitution and crystallinity in biogenic hydroxyapatite: Dentin and enamel in normal and hypoplastic human teeth. *Journal of Raman Specroscopy*, *49*, 1559–1567.

74. Aldred, M. J., Crawford, P. J. M., Rowe, W., Rowe, W., & Shellis, R. P. (1992). Scanning electron-microscopic study of primary teeth in X-linked *Amelogenesis imperfecta*. *Journal of Oral Pathology & Medicine*, *21*, 186–192.

75. Coyac, B. R., Falgayrac, G., Penel, G., Schmitt, A., Schinke, T., Linglart, A., Mckee, M. D., Chaussain, C., & Bardet, C. (2018). Impaired mineral quality in dentin in X-linked hypophosphatemia. *Connective Tissue Research*, *59*, 91–96.

76. BÃrjesson, J., & Mattsson, S. (2007). Medical applications of X-ray fluorescence for trace element research. *Powder Diffraction*, *22*, 130–137.

77. Macdonald, N. S., Noyes, P., & Lorick, P. C. (1957). Discrimination of calcium and strontium by the kidney. *American Journal of Physiology*, *188*, 131–136.

78. Oâdonnell, M. D., Fredholm, Y., De Rouffignac, A., & Hill, R. G. (2008). Structural analysis of a series of strontium-substituted apatites. *Acta Biomaterialia*, *4*, 1455–1464.

79. Pan, H. B., Li, Z. Y., Lam, W. M., Wong, J. C., Darvell, B. W., Luk, K. D. K., & Lu, W. W. (2009). Solubility of strontium-substituted apatite by solid titration. *Acta Biomaterialia*, *5*, 1678–1685.

80. Dahl, S. G., Allain, P., Marie, P. J., Mauras, Y., Boivin, G., Ammann, P., Tsouderos, Y., Delmas, P. D., & Christiansen, C. (2001). Incorporation and distribution of strontium in bone. *Bone*, *28*, 446–453.

81. Martins, C. C., Firmino, R. T., Riva, J. J., Ge, L., Carrasco-Labra, A., Brignardello-Petersen, R., Colunga-Lozano, L. E., Granville-Garcia, A. F., Costa, F. O., Yepes-Nuñez, J. J., Zhang, Y., & Schünemann, H. J. (2020). Desensitizing toothpastes for dentin hypersensitivity: A network meta-analysis. *Journal of Dental Research*, *99*, 514–522.

82. Van Den Berkhof, Y. S., Gant, C. M., Maatman, R., De Graaf, A., Navis, G. J., Bakker, S. J. L., & Laverman, G. D. (2018). Correlations between plasma strontium concentration, components of calcium and phosphate metabolism and renal function in type 2 diabetes mellitus. *European Journal of Clinical Investigation*, *48*, e12987.

83. Vezzoli, G., Baragetti, I., Zerbi, S., Caumo, A., Soldati, L., Bellinzoni, P., Centemero, A., Rubinacci, A., Moro, G., & Bianchi, G. (1998). Strontium absorption and excretion in normocalciuric subjects: Relation to calcium metabolism. *Clinical Chemistry*, *44*, 586–590.

84. Jalali, R., Lodder, J. C., Zandieh-Doulabi, B., Micha, D., Melvin, J. E., Catalan, M. A., Mansvelder, H. D., Denbesten, P., & Bronckers, A. (2017). The role of Na:K:2Cl cotransporter 1 (NKCC1/SLC12A2) in dental epithelium during enamel formation in mice. *Frontiers in Physiology*, *8*, 924.

85. Yin, K., & Paine, M. L. (2017). Bicarbonate transport during enamel maturation. *Calcified Tissue International*, *101*, 457–464.

86. Parry, D. A., Mighell, A. J., El-Sayed, W., Shore, R. C., Jalili, I. K., Dollfus, H., Bloch-Zupan, A., Carlos, R., Carr, I. M., Downey, L. M., Blain, K. M., Mansfield, D. C., Shahrabi, M., Heidari, M., Aref, P., Abbasi, M., Michaelides, M., Moore, A. T., Kirkham, J., & Inglehearn, C. F. (2009). Mutations in CNNM4 cause Jalili syndrome, consisting of autosomal-recessive cone-rod dystrophy and *Amelogenesis imperfecta*. *American Journal of Human Genetics*, *84*, 266–273.

87. Jälevik, B., Odelius, H., Dietz, W., & Norén, J. (2001). Secondary ion mass spectrometry and X-ray microanalysis of hypomineralized enamel in human permanent first molars. *Archives of Oral Biology*, *46*, 239–247.

88. Aoba, T., Shimoda, S., & Moreno, E. C. (1992). Labile or surface pools of magnesium, sodium, and potassium in developing porcine enamel mineral. *Journal of Dental Research*, *71*, 1826–1831.

89. Bronckers, A. L. J. J., Jalali, R., & Lytton, J. (2017). Reduced protein expression of the Na(+)/Ca(2+)+K(+)-exchanger (SLC24A4) in apical plasma membranes of maturation ameloblasts of fluorotic mice. *Calcified Tissue International*, *100*, 80–86.

90. Khandelwal, P., Sabanadesan, J., Sinha, A., Hari, P., & Bagga, A. (2020). Isolated nephrocalcinosis due to compound heterozygous mutations in renal outer medullary potassium channel. *CEN Case Report*, *9*, 232–236.

91. Kumar, A. C. V., Alekya, V., Krishna, M., Alekya, K., Aruna, M., Reddy, M. H. K., Sangeetha, B., Ram, R., & Kumar, V. S. (2017). Association of *Amelogenesis imperfecta* and Bartter's syndrome. *Indian Journal of Nephrology*, *27*, 399–401.

SUPPORTING INFORMATION

Additional supporting information can be found online in the Supporting Information section at the end of this article.